minerals

MDPI

Article

Crystal Structure Evolution of $CaSiO_3$ Polymorphs at Earth's Mantle Pressures

Sula Milani [1,*], Davide Comboni [2], Paolo Lotti [1], Patrizia Fumagalli [1], Luca Ziberna [3], Juliette Maurice [1], Michael Hanfland [2] and Marco Merlini [1]

[1] Dipartimento di Scienze della Terra 'Ardito Desio', Università degli Studi di Milano, Via Botticelli 23, 20133 Milan, Italy; paolo.lotti@unimi.it (P.L.); patrizia.fumagalli@unimi.it (P.F.); juliettemaurice@gmail.com (J.M.); marco.merlini@unimi.it (M.M.)

[2] ESRF-European Synchrotron Radiation Facility, 71 Avenue des Martyrs, CS40220, CEDEX 09, 38043 Grenoble, France; davide.comboni@esrf.fr (D.C.); hanfland@esrf.fr (M.H.)

[3] Dipartimento di Matematica e Geoscienze, Università degli Studi di Trieste, Via Weiss 8, 34128 Trieste, Italy; luca.ziberna@units.it

* Correspondence: sula.milani@unimi.it

Abstract: $CaSiO_3$ polymorphs are abundant in only unique geological settings on the Earth's surface and are the major Ca-bearing phases at deep mantle condition. An accurate and comprehensive study of their density and structural evolution with pressure and temperature is still lacking. Therefore, in this study we report the elastic behavior and structural evolution of wollastonite and $CaSiO_3$-walstromite with pressure. Both minerals are characterized by first order phase transitions to denser structures. The deformations that lead to these transformations allow a volume increase ofthe bigger polyhedra, which might ease cation substitution in the structural sites of these phases. Furthermore, their geometrical features are clear analogies with those predicted and observed for tetrahedrally-structured ultra-high-pressure carbonates, which are unfortunately unquenchable. Indeed, wollastonite and $CaSiO_3$-walstromite have a close resemblance to ultra-high-pressure chain- and ring-carbonates. This suggests a rich polymorphism also for tetrahedral carbonates, which might increase the compositional range of these phases, including continuous solid solutions involving cations with different size (Ca vs. Mg in particular) and important minor or trace elements incorporation.

Keywords: $CaSiO_3$ polymorphs; mineral physics; elastic properties; crystal structure; carbonates

Citation: Milani, S.; Comboni, D.; Lotti, P.; Fumagalli, P.; Ziberna, L.; Maurice, J.; Hanfland, M.; Merlini, M. Crystal Structure Evolution of $CaSiO_3$ Polymorphs at Earth's Mantle Pressures. *Minerals* **2021**, *11*, 652. https://doi.org/10.3390/min11060652

Academic Editor: Hans-Rudolf Wenk

Received: 27 May 2021
Accepted: 11 June 2021
Published: 19 June 2021

1. Introduction

Calcium is the 13th most abundant element in our solar system [1]. Indeed, on our planet, it is one of the rock forming elements and its abundance in Earth bulk composition is about ca. 1.71%, considering an approximate mass of the Earth of 5.98×10^{24} kg [2]. Ca abundance on the Earth's crust is about 6.4 wt% [3], while in the Earth's mantle, it is ca. 26,100 ppm [4]. For this reason, the study of Ca bearing minerals, might shade new light on the redistribution of this element on and in the Earth. Calcium is mainly hosted in calcium carbonates and in several rock-forming minerals such as feldspars, pyroxenes and amphiboles. In addition, pure calcium silicates, such as $CaSiO_3$ polymorphs are of paramount relevance in only unique geological settings, such as skarns formed at metamorphic reaction zones due to the interplay between carbonate- and silicate-based lithologies.

Wollastonite and breyite (previously labelled as $CaSiO_3$-walstromite) form in magmatic and/or metamorphic environments, and represent the low-pressure and low-temperature polymorphs of the Ca-perovskite [5]. The latter is the major Ca-bearing phase in the lower mantle and the fourth most abundant mineral at these conditions [6,7].

$CaSiO_3$ polymorphism is of particular interest for their peculiar crystal chemical features. The geometrical features observed in chain and ring-structured $CaSiO_3$ minerals present in fact clear analogies with the predicted and observed features in tetrahedrally-structured ultra-high-pressure carbonates [8]. In the past, due to analytical difficulties

to study the occurrence of phase transformation in silicates at extreme conditions, the investigation of germanates has been adopted as structural analogues of silicates at high pressures [9]. Indeed, germanates transforms to new denser phases at much lower pressures compared to isostructural silicates [9]. The same approach can be applied to study the unquenchable sp^3 polymorphs with tetrahedrally-coordinated carbon, using in this case selected silicates as structural analogues. Bearing in mind that the structural variety of tetrahedral carbonates is much lower with respect to the enormous diversity in silicate structures [10], it is worth of notice the closed resemblance of ultra-high-pressure chain- and ring-carbonates with topological features in wollastonite and breyite. Carbonate minerals are considered as one of the main carbon host phases in the mantle. They are stable from crust to lower mantle, as demonstrated by direct observation of carbonate inclusions in superdeep diamonds [11]. To date, the different possible structures adopted by carbonates during their polymorphic phase transitions are still unclear [12], even if recent experimental [13] and theoretical studies [14] have demonstrated the transformation into complex tetrahedral ring or chain carbonate structures. Given the unquenchable character of ring-carbonates and the difficulties in performing high pressure single crystal diffraction with suitable quality of data for accurate structural details determination, $CaSiO_3$ system constitutes an interesting proxy to understand crystal chemistry implication of possible variability in high-pressure carbonate structures. Nonetheless, $CaSiO_3$ analogues could play a key-role to improve the understanding of the evolution of the tetrahedrally-coordinated carbonates at extreme conditions and could be paramount to unravel the deep carbon cycle in the deepest parts of the Earth and on other planets.

In this article, we report the results of experimental investigations on the structural evolution of wollastonite and $CaSiO_3$-walstromite (breyite) phases under high-pressures by single crystal synchrotron X-ray diffraction. The results provide new valuable data on $CaSiO_3$ polymorphism and crystal chemical evolution at mantle pressures.

Polymorphism and Polytypism in $CaSiO_3$ System up to ca. 8 GPa

The polymorphism and polytypism of the calcium metasilicate system has been studied since the late 19th century and received a new influx after the application of X-ray measurements in mineralogy. The calcium metasilicate system is characterized by several phases stable over a wide range of temperature and pressure, reaching the deepest parts of the lower Earth's mantle (Figure 1).

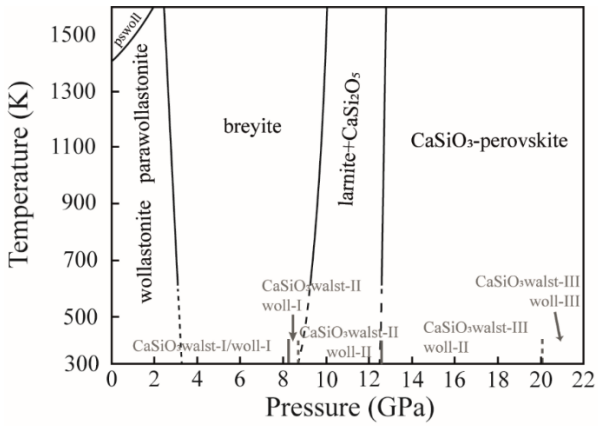

Figure 1. Phase diagram of the system $CaSiO_3$. Lines for the wollastonite, breyite fields have been calculated using elastic parameters determined in this paper, the other data have been taken from [15].

Wollastonite is a Ca-rich silicate and a rock forming mineral in the upper crust [16]. It is characterized by two polymorphs (α- and β-wollastonite) and each polymorph is characterized by few polytypes. β-wollastonite or better determined as wollastonite is a chain-silicate and its structure consists of infinitely long single chains, running along the *b* axis characterized by a periodicity of three. These chains are composed by a couple

of two silicon tetrahedra, Si_2O_7, paired to one silicon tetrahedron, SiO_4 (Figure 2a). The chains are linked by Ca cations, located in octahedrally distorted polyhedra (Figure 2a). In the tetrahedra minor substitution of Si with Al might occur, while in the octahedron large substitution of Ca with Mg, Mn, and Fe^{2+} are possible. The two most abundant and common polytypes in nature are wollastonite (1*T* wollastonite; Figure 2a and Table 1) and wollastonite-2*M* (parawollastonite; Figure 2b and Table 1).

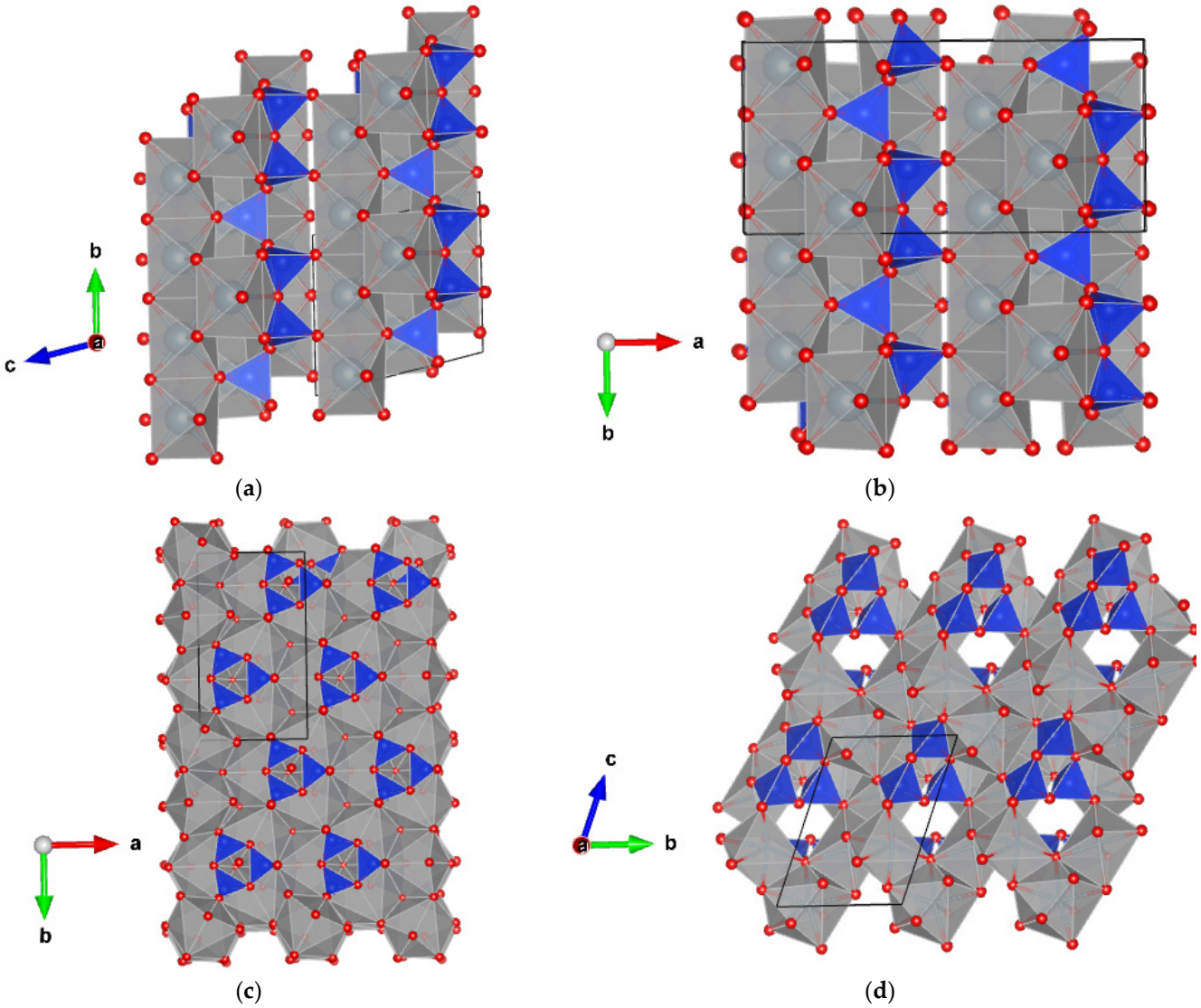

Figure 2. Crystal structure of (**a**) wollastonite, (**b**) wollastonite-2*M*, (**c**) pseudowollastonite, and (**d**) breyite. The representations of the structure are realized using the program VESTA [17]. Small red spheres are oxygens, $(SiO_4)^{2-}$ are blue tetrahedra and grey polygons are Ca cation sites. Black solid lines represent the dimension of the unit cell.

Table 1. Unit-cell constants of $CaSiO_3$ system up to ca. 8 GPa.

Phase	*a* (Å)	*b* (Å)	*c* (Å)	*α* (°)	*β* (°)	*γ* (°)	Space Group	Reference
wollastonite	7.079(2)	7.3309(4)	7.938(2)	103.41(2)	95.30(2)	90.07 (2)	$P\bar{1}$	This study
wollastonite-2*M*	15.409(3)	7.322(1)	7.063(1)	90	95.30(2)	90	$P2_1/a$	[18]
pseudowollastonite	6.8394(5)	11.8704(9)	19.6313(7)	90	90.667(6)	90	$C2/c$	[19]
$CaSiO_3$-walstromite	6.6442(4)	6.6886(4)	9.282(8)	69.71(3)	83.68(2)	76.21(1)	$P\bar{1}$	This study

Wollastonite belongs to the triclinic system, while wollastonite-2*M* belongs to the monoclinic one. They are mostly found in contact metamorphic limestones (e.g., Bazena

Alps, Finish Archean metamorphic calcitic limestones, Namaqua Metamorphic Complex, Crestmore) as a product from the reaction of calcite and quartz [20]. Other occurrences are as inclusions in feldspar, nepheline and aegirine from nepheline syenite [21] or as secondary product after plagioclase [21]. Wollastonite and wollastonite-2*M*, because of their small structural energy difference, [22] occur together, with a predominant occurrence of wollastonite. In few exceptions, wollastonite-2*M* is more abundant, like in M.te Somma (Campania, Italy) rocks. Wollastonite and wollastonite-2*M* are closely related, because of the so called 'space-group twinning' [23–26]. Indeed this 'twinning' stacks, in different modes, a pseudomonoclinic subcell along the direction of *a*-axis, forming a triclinic or a monoclinic asymmetry. In the literature, these different stacking modes have been observed in other polytypes (3*T*, 4*T* and 5*T*) discovered near Kushiro (Hokkaidō Region, Japan; [27]). This group of minerals can occur as elongated prismatic crystals, and they are usually transparent to translucent; the lustre varies from vitreous to pearly and, in general, these minerals are characterized by a perfect cleavage on (001). They can occur in many different colors (e.g., yellow, red, light green, brown, and pink), but they are more frequently white or grey-white. The high-temperature ambient pressure polymorph of wollastonite, stable above ca. 1125 °C, is the pseudowollastonite or α-wollastonite (Figure 1). Historically it was thought that pseudowollastonite was stable only as a synthetic mineral because it was found only as a common product in slags, cement and ceramic materials and it was common in petrological experiments. Indeed, in nature pseudowollastonite is very rare and up to date it has been reported only in three localities: Chillingar oilfield (Iran) and two areas located in the so-called Mottled Zone complexes (Israel). The rocks that contain the pseudowollastonite are the so-called Ca-rich combustion metamorphic rocks (paralavas and hornfels), which formed in ultra-high temperature and very low-pressure environment, due to spontaneous ignition of high-calorific hydrocarbons [28]. Pseudowollastonite was also reported as a rare phase in mantle-derived melilitolite from Colle Fabbri (Italy; [29]). Pseudowollastonite is a cyclosilicate characterized by a layered structure. Indeed, layers of ternary rings, Si_3O_9, are perpendicular to *c* axis, and they are connected by layers of octahedrally coordinated Ca-polyhedra (Figure 2c; [19]). Until 2012, pseudowollastonite was studied only *via* synthetic samples, which showed several polytypes due to the different stacking sequences of the displaced layers of ternary silicate rings. A monoclinic polytype was described by [19], characterized by a 4-layered structure, while the experiments done by [30] obtained the coexistence of three distinct polytypes (2-, 4-, and 6-layered), due to different experimental procedures. In 2012, a first study based on natural pseudowollastonite was published [28]. As it was already experimentally predicted, [16] natural pseudowollastonite is a stoichiometric $CaSiO_3$ compound [28], while wollastonite can incorporate up to 10 mol% of $FeSiO_3$ and $MgSiO_3$. The structure of the natural pseudowollastonite belonged to the most common four-layered polytype characterized by a monoclinic symmetry in the space group *C2/c* [28].At pressure above 3 GPa another ring silicate is stable, and this $CaSiO_3$-walstromite is the synthetic analogue for breyite mineral [31]. $CaSiO_3$-walstromite is stable over a wide range of pressures and temperatures (Figure 1). In the last decades $CaSiO_3$-walstromite has become paramount to the understanding of the deep Earth's upper mantle because Ca-silicate polymorphs such as $CaSiO_3$-walstromite, titanite structured $CaSi_2O_5$ and larnite (Ca_2SiO_4) were found as inclusions in diamonds [32,33] being the evidence of a Ca-rich lithology in the Earth's mantle. Recently $CaSiO_3$-walstromite, being the second most abundant mineral inclusion found in super-deep diamonds, has been named breyite [34,35]. In the past, breyite was referred to $CaSiO_3$-walstromite because of the similar crystal structure to walstromite ($Ca_2BaSi_3O_9$). Walstromite as well as breyite belong to the triclinic symmetry, with a $P\bar{1}$ space group (Figure 2d; Table 1). $CaSiO_3$-walstromite is characterised by layers of Si_3O_9 rings connected by layers of octahedrally coordinated Ca parallel to each other [36]. Also, breyite composition, as the lower pressure polymorph, is characterized by only CaO and SiO_2 [34]; in the literature, FeO is the main impurity of breyite, reported to occur only in low percentages [37].

For the sake of completeness, we also report a high-pressure phase of wollastonite, named wollastonite-II [38]. It was first considered as a polytype of walstromite, but it has been demonstrated that walstromite, $CaSiO_3$-walstromite, and wollastonite-II are all isomorphs [39]. In the following discussion, we will refer to $CaSiO_3$-walstromite, to indicate the synthetic nature of the material investigated, and to breyite for general implications. In this context we will use the term wollastonite-II to be referring to the first transition of wollastonite at higher pressures.

2. Materials and Methods

Synthetic large single crystals (up to 150 μm × 80 μm × 80 μm) of pure $CaSiO_3$-walstromite ($CaSiO_3$) were obtained at high pressure and high temperature using a multi-anvil module at the 'Dipartimento di Scienze della Terra, A. Desio', University of Milan (DES-UM). A gel of stoichiometric $CaSiO_3$ composition was used as starting material prepared following the procedure adopted by [40]. Platinum capsules (3.5 mm length and 2 mm diameter) were welded after being loaded with the gel and saturated with bi-distilled water, which was added with a micro-syringe. Cr-doped MgO octahedra of 25 mm of edge length were used as pressure cell in 32 mm edge length tungsten carbide cubes. Graphite heaters were used, and temperatures were measured by a Pt-PtRh thermocouple (S-type). Temperature is accurate to ±20 K, with no pressure correction for e.f.m. of thermocouple. Pressure uncertainties were assumed ±3% according to the accuracy of calibrant reactions [41]. Samples of $CaSiO_3$-walstromite were synthesized at 6 GPa and 1773 K (ramp rate at about 39 K/min) with a run duration of 6 h, after this dwell, the temperature was decreased to 1673 K and quenched after 48 h. The multi-anvil experiment was performed with a Cr-doped MgO octahedron of 25 mm edge length combined with tungsten carbide cubes of 15 mm truncation-edge lengths. All run products were characterized via preliminar conventional single crystal X-ray diffraction measurements.

Wollastonite single crystals were recovered from rock samples kindly provided by the Museum of Mineralogy of the DES-UM. The sample is from Bazena Alp, Breno (BS), Italy [20]. The chemical composition of the sample has been determined by chemical microanalyses in wavelength-dispersive mode (EPMA-WDS) at DES-UM using a Jeol 8200 operating at 15 nA and 15 kV with standard of grossular for both Si and Ca.

In-situ HP single crystal X-ray diffraction experiments were done at beamlines ID09 and ID15b at the European Synchrotron Radiation Facility (ESRF, Grenoble, France). A convergent monochromatic beam (E~30 keV, λ~0. 4110 and 0.4112 Å respectively) was used for the diffraction experiment. Single crystal diffraction data were collected by phi scans in the angular range ±38 with step size of 0.5°. The diffraction patterns were collected by a MAR555 flat-panel detector, positioned at about 280 mm from the sample position. Sample-to-detector distance was calibrated using a Si powder standard 640b SRM (NIST) and a pure enstatite ($MgSiO_3$) crystal. The details on the beamlines setup are reported in [42]. Single crystals of natural wollastonite and pure $CaSiO_3$-walstromite (ca. 20 μm × 20 μm × 10 μm) were loaded in two different membrane-driven DACs (Diamond Anvil Cells), with 600 μm culet Boehler-Almax design anvils, along with a few ruby spheres for P-determination (pressure uncertainty ±0.05 GPa [43,44]). The pressure chamber was created placing a Re gasket pre-indented to 80 μm thickness and drilling a hole of ca. 100 μm by a spark eroder. DACs were loaded with He gas as pressure transmitting medium, which transmits pressure hydrostatically up to the maximum pressures reached in this study of about ca. 20 GPa in both the experiments [45]. Data were indexed and integrated with Crysalis Red Software [46], after being converted following the established protocols for the beamlines [42]. Lorenz-polarization and absorption correction were applied using the semi-empirical ABSPACK routine implemented in CrysAlis. The structural solution and the structural refinement for each HP point were handled with Jana software [47].

3. Results

3.1. High-Pressure Polytypes of Wollastonite

Single crystal data of wollastonite at high pressure are indexed with the ambient pressure triclinic unit cell up to ca. 8.3 GPa. At higher pressures, up to ca. 19.2 GPa, new peaks appear, and the diffractions are indexed with a 1 × 1 × 2 supercell. Above 19.2 GPa, the diffractions are indexed with a 1 × 2 × 2 supercell. These observations indicate two phase transitions, and the three phases are named wollastonite-I, wollastonite-II and wollastonite-III.

The evolution of the unit-cell volume of wollastonite at different pressures (P) is reported in Table 2 and Figure 3. The volume decreases smoothly with increasing pressure, as shown in Figure 3, up to ca. 8 GPa. As it can be observed, the wollastonite-I to wollastonite-II phase transition is a first-order transition, evidenced by the marked volume discontinuity present in the data above 8.2 GPa, with a volume change of approx. 5%. The second phase transition wollastonite-II to wollastonite-III is a likely second-order phase transition, with negligible volume change upon transitions. P–V data were fitted using the program EoSFit-7c [48]. P–V data up to 8 GPa were fitted using a second-order Birch–Murnaghan EoS (BM2-EoS; [49]), since the Eulerian finite strain (f_e) vs. normalized stress (F_e) plot of the data can be fitted by a horizontal straight line [50]. The BM2-EoS coefficients were refined simultaneously, data were weighted by their uncertainties in P and V giving: V_0 = 398.7(2) Å^3, K_{T0} = 93.9(8) GPa and K' = 4 fixed (χ^2_w = 1.01 and ΔPmax = −0.25 GPa). The V data in the pressure range where the 2nd phase transition is stable (9.3–19.2 GPa) decreases smoothly (Figure 3). The P–V were fitted using a BM2-EoS [49]. The refined bulk modulus is K_{T0} = 78.2(3) GPa (K' = 4 fixed). Since the 3rd phase transition has been measured by only four datapoints, no EoS parameters have been estimated due to a lack of data (Figure 3).

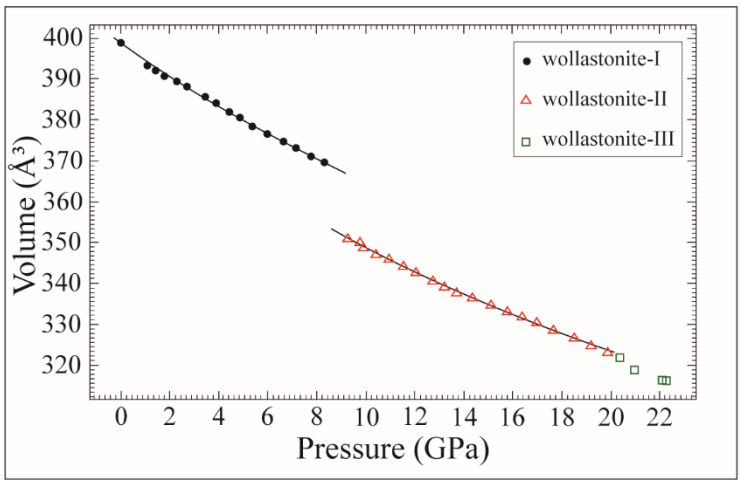

Figure 3. Evolution of the unit-cell volume with pressure of wollastonite. Unit-cell volume data of the two HP polytypes have been normalized to the low-P polytype. The solid line represents the 2nd order BM-EoS fit.

The single crystal X-ray diffraction measurement confirms a triclinic structure, with $P\bar{1}$ symmetry for all the three polytypes. The refined unit-cell parameters of wollastonite-I at ambient conditions are a = 7.0786(16), b = 7.3309(4), c = 7.938(2) Å, α= 103.41(2), β = 95.30(2), γ = 90.07(2) and V = 398.87(13) Å^3. The refined unit cell parameters for all the pressure points for the three polytypes are listed in Table 2. Structure solution for both wollastonite-II and wollastonite-III reveals the main topological features and the relationship between these polytypes. The crystal structure was solved and refined at different pressures using the crystallographic software Jana2006 [47]. The principal statistical parameters of the three structural refinements are listed in Table 3. Atomic coordinates, site occupancies of structure

refinements, and relevant bond distances are reported in Tables S1 and S2 (Supplementary Materials). The crystallographic information file is available as Supplementary Materials.

Table 2. Lattice parameters of wollastonite at different pressures, collected using helium as *P*-transmitting medium (*P*-uncertainty: ±0.05 GPa).

P (GPa)	*a* (Å)	*b* (Å)	*c* (Å)	*α* (°)	*β* (°)	*γ* (°)	*V* (Å^3)
wollastonite-I							
0.0001	7.079(2)	7.3309(4)	7.938(2)	103.41(2)	95.30(2)	90.07(2)	398.9(2)
1.08	7.049(3)	7.3105(4)	7.901(3)	103.44(2)	95.12(3)	90.04(2)	393.3(2)
1.44	7.030(3)	7.3054(4)	7.882(3)	103.45(2)	94.96(3)	90.04(2)	392.1(2)
1.78	7.022(3)	7.2990(4)	7.871(3)	103.45(2)	94.92(3)	90.04(2)	390.8(2)
2.29	7.015(3)	7.2905(5)	7.858(3)	103.46(2)	94.91(3)	90.03(2)	389.3(2)
2.72	7.007(3)	7.2833(4)	7.850(3)	103.46(2)	94.88(3)	90.01(2)	388.1(2)
3.45	6.991(3)	7.2717(3)	7.828(2)	103.47(2)	94.77(3)	90.00(2)	385.6(2)
3.90	6.983(2)	7.2645(4)	7.814(2)	103.48(2)	94.70(3)	90.00(2)	384.1(2)
4.43	6.969(2)	7.2556(4)	7.797(2)	103.49(2)	94.59(3)	89.99(2)	382.1(2)
4.86	6.958(2)	7.2478(3)	7.783(2)	103.50(2)	94.50(3)	89.99(2)	380.4(2)
5.38	6.947(2)	7.2390(3)	7.766(2)	103.52(2)	94.39(3)	89.98(2)	378.6(2)
5.97	6.934(2)	7.2300(3)	7.750(2)	103.53(1)	94.27(2)	89.97(1)	376.6(2)
6.62	6.922(2)	7.2202(4)	7.731(2)	103.55(2)	94.11(2)	89.95(2)	374.7(2)
7.16	6.914(2)	7.2127(4)	7.716(2)	103.58(2)	94.00(2)	89.93(2)	373.1(2)
7.75	6.904(2)	7.2033(3)	7.699(2)	103.59(1)	93.83(2)	89.94(1)	371.3(2)
8.29	6.895(2)	7.1945(3)	7.684(2)	103.62(1)	93.66(2)	89.92(1)	369.6(3)
wollastonite-II							
9.27	6.693(2)	7.2561(3)	14.927(9)	76.048(9)	86.95(2)	89.951(9)	702.5(3)
9.76	6.696(2)	7.2461(3)	14.896(4)	76.06(1)	86.94(2)	89.99(2)	700.3(3)
9.91	6.679(2)	7.2509(5)	14.872(2)	76.012(9)	87.11(2)	89.966(9)	697.9(2)
10.13	6.647(2)	7.2183(4)	14.786(4)	76.00(2)	87.26(2)	89.98(2)	687.6(3)
10.42	6.671(2)	7.2430(4)	14.835(4)	76.00(2)	87.21(2)	89.98(2)	694.6(3)
10.94	6.668(2)	7.2371(3)	14.799(2)	75.977(7)	87.23(2)	89.984(7)	692.1(2)
11.54	6.659(2)	7.2314(3)	14.762(2)	75.956(7)	87.33(2)	89.990(8)	688.8(2)
12.06	6.653(2)	7.2245(4)	14.721(4)	75.96(1)	87.42(2)	90.01(1)	685.6(3)
12.34	6.670(2)	7.2239(5)	14.724(4)	75.94(2)	87.30(3)	90.02(2)	687.4(3)
12.75	6.644(2)	7.2163(2)	14.673(2)	75.927(6)	87.49(2)	90.001(7)	681.7(2)
13.21	6.638(2)	7.2108(2)	14.640(2)	75.907(6)	87.56(2)	90.005(7)	679.0(2)
13.71	6.631(2)	7.2046(2)	14.604(2)	75.887(6)	87.65(2)	90.007(7)	676.0(2)
14.37	6.626(2)	7.1975(3)	14.568(2)	75.870(6)	87.70(2)	90.015(7)	673.1(2)
15.11	6.620(2)	7.1899(3)	14.525(2)	75.849(7)	87.79(2)	90.027(7)	669.8(2)
15.78	6.615(2)	7.1835(3)	14.486(2)	75.831(6)	87.87(2)	90.037(8)	666.9(2)
16.38	6.609(2)	7.1783(3)	14.449(2)	75.802(6)	87.93(2)	90.038(7)	664.0(2)
16.98	6.604(2)	7.1733(2)	14.411(2)	75.768(6)	87.99(2)	90.046(6)	661.3(2)
17.67	6.594(2)	7.1688(3)	14.366(2)	75.729(6)	88.07(2)	90.061(7)	657.7(2)
18.50	6.587(2)	7.1632(3)	14.313(2)	75.670(6)	88.23(2)	90.038(7)	654.0(2)
19.20	6.578(2)	7.1587(3)	14.259(2)	75.627(6)	88.44(2)	90.023(7)	650.2(2)
19.85	6.575(2)	7.1563(3)	14.200(2)	75.556(6)	88.60(2)	90.032(7)	646.8(2)
wollastonite-III							
20.39	6.571(2)	14.142(2)	14.3107(5)	75.488(6)	89.967(7)	91.22(2)	1287.1(3)
20.98	6.568(2)	14.012(2)	14.3262(5)	75.324(6)	89.834(7)	90.81(2)	1275.3(3)
22.11	6.561(2)	13.925(2)	14.3264(5)	75.237(6)	89.789(7)	90.61(2)	1265.5(3)
22.29	6.564(2)	13.910(3)	14.3224(6)	75.222(7)	89.850(7)	90.62(2)	1264.3(3)

The main structural units of wollastonite structure are the silicate chains, with 3-fold periodicity. The tetrahedral non-bridging oxygens are chemically bonded to calcium, which is in variable coordination polyhedra (6-7-fold coordination polyhedra). One structural change upon wollastonite-I to wollastonite-II transition is a slight rotation of the tetrahedral, without affecting chain periodicity. The major structural change, which is responsible of the significant density increase of the structure, is a translation of two silicon chains along the *b*-axis (Figure 4a,b). The periodicity along the *c*-axis is therefore described by four chains instead of two (Figure 2b) leading to a doubling of the unit-cell value in this

direction (Table 2). These changes are also visible on the dramatic volume increase of two 6-coordinated polyhedral (Figure S1). The phase transition from wollastonite-II to wollastonite-III involves the rotation of SiO_4 tetrahedra within the chains, with an increase in periodicity from three to six tetrahedra. The topology of wollastonite-III is similar to wollastonite-II, therefore no volume jump is observed, but only a doubling of the unit-cell value along the elongation of tetrahedral chains (Figure 4b,c).

Table 3. Details pertaining to the data collections and structure refinements of wollastonite studied in this work.

Phase	Wollastonite-I	Wollastonite-II	Wollastonite-III
a (Å)	7.079(2)	6.693(2)	6.571(2)
b (Å)	7.3309(4)	7.2561(3)	14.142(2)
c (Å)	7.938(2)	14.9270(3)	14.3107(5)
α (°)	103.41(2)	76.048(9)	75.488(6)
β (°)	95.29(2)	86.95(2)	89.967(7)
γ (°)	90.07(2)	89.951(9)	91.22(2)
V (Å^3)	398.9(2)	702.5(3)	1287.1(3)
P (GPa)	0.0001(1)	9.27(5)	20.39(5)
Space group	$P\bar{1}$	$P\bar{1}$	$P\bar{1}$
λ (Å)	0.41105	0.41105	0.41105
θ_{max} (°)	18.51	18.43	18.42
No. measured reflections	1216	2206	12838
No. unique reflections	766	1426	3184
No. refined parameters	61	121	241
R_{int}	0.028	0.0488	0.1711
R_1 (F)	0.0493	0.0657	0.0816
wR_2 (F^2)	0.0604	0.0790	0.0882
GooF	3.74	3.92	3.47
Residuals (e$^-$/Å^3)	−5.10/+10.36	−1.40/+1.42	−2.41/+7.54

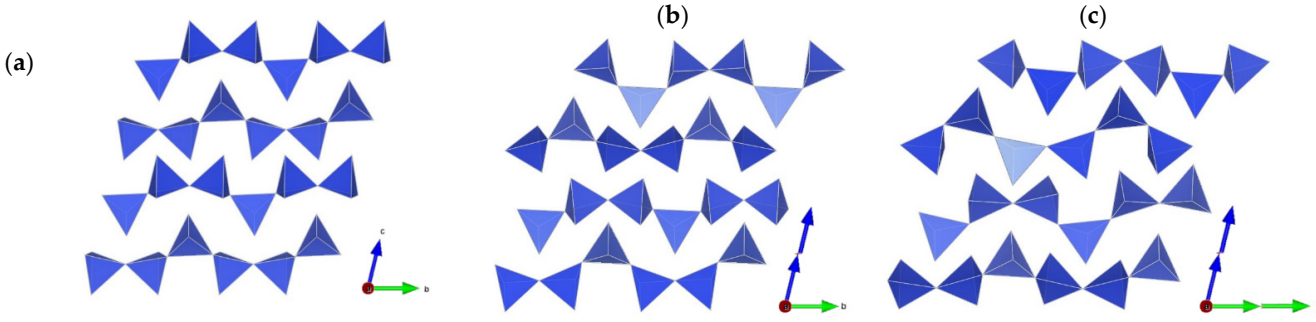

Figure 4. Phase transitions from (**a**) wollastonite-I (**b**) wollastonite-II and (**c**) wollastonite-III. The representations of the structure are realized using the program VESTA [17]; a axis points toward the reader, the green arrow is the b axis, while the blue arrow is the c axis. The blue and the green axis are doubled in (**b**,**c**) as it can be observed from the unit-cell parameters of the two polytypes (Table 3).

3.2. High-Pressure Polytypes of $CaSiO_3$-Walstromite

The evolution of the unit-cell volume of $CaSiO_3$-walstromite at different P is reported in Table 4 and Figure 5. The volume decreases smoothly with increasing pressure, as shown in Figure 5, up to ca. 8.5 GPa, afterwards two phase transitions occur in the structure within the P-range investigated. The first phase transition, from $CaSiO_3$-walstromite-I to $CaSiO_3$-walstromite-II, is marked by a change in crystal lattice and symmetry, from a triclinic unit cell and $P\bar{1}$ space group, to a monoclinic C-centred lattice. The second phase transition, from $CaSiO_3$-walstromite-II to $CaSiO_3$-walstromite-III, is marked by a change in lattice-type; the unit cell is the same as $CaSiO_3$-walstromite-II but the lattice

is primitive. As it can be observed from Figure 5, the first phase transition is clearly a first-order transition, evidenced by the volume discontinuity of ca. 3% present in the data at ca. 8.5 GPa. A "jumping crystal" effect [51] upon transition is noticeable (Figure S2), which is also visible during decompression.

Table 4. Lattice parameters of $CaSiO_3$-walstromite at different pressures, collected using helium as *P*-transmitting medium (*P*-uncertainty: ±0.05 GPa).

P (GPa)	*a* (Å)	*b* (Å)	*c* (Å)	*α* (°)	*β* (°)	*γ* (°)	*V* (Å^3)
			$CaSiO_3$-walstromite-I				
0.0001	6.6442(3)	6.6886(4)	9.282(8)	69.71(3)	83.68(2)	76.205(5)	375.6(3)
1.39 [d]	6.605(3)	6.6457(6)	9.230(4)	69.99(3)	83.45(4)	76.41(3)	369.8(2)
1.71 [d]	6.591(2)	6.6347(5)	9.213(3)	70.03(2)	83.45(3)	76.45(2)	367.9(2)
2.60 [d]	6.573(2)	6.6109(6)	9.186(3)	70.14(2)	83.28(3)	76.55(2)	364.8(2)
3.45 [d]	6.550(2)	6.5911(7)	9.156(3)	70.21(2)	83.25(2)	76.63(2)	361.5(2)
4.76 [d]	6.514(2)	6.5592(8)	9.114(3)	70.28(2)	83.16(2)	76.73(2)	356.4(2)
6.02	6.4908(3)	6.5385(3)	9.087(5)	70.28(2)	83.03(2)	76.804(5)	353.1(2)
6.60 [d]	6.468(2)	6.5156(7)	9.061(3)	70.36(2)	82.97(3)	76.87(2)	349.8(2)
6.97	6.4602(3)	6.5084(3)	9.018(7)	70.34(3)	82.89(2)	76.874(5)	347.3(3)
7.68	6.4445(4)	6.4935(3)	9.009(6)	70.38(2)	82.82(2)	76.919(5)	345.4(3)
8.48	6.4273(3)	6.4777(3)	9.007(5)	70.41(2)	82.77(2)	76.970(4)	343.7(2)
			$CaSiO_3$-walstromite-II				
7.84 [d]	10.2206(9)	7.9369(9)	8.6213(7)	90	105.217(9)	90	674.8(4)
8.77 [d]	10.1897(2)	7.9217(2)	8.5966(2)	90	105.137(2)	90	669.8(4)
9.37	10.1649(2)	7.9143(3)	8.5806(2)	90	105.098(2)	90	666.5(5)
9.37 [d]	10.1707(4)	7.9119(5)	8.5811(3)	90	105.087(4)	90	666.7(4)
9.75 [d]	10.1613(2)	7.9078(2)	8.5745(2)	90	105.057(2)	90	665.3(3)
10.23	10.1432(3)	7.9020(3)	8.5629(2)	90	104.9817(2)	90	663.0(4)
11.10 [d]	10.1208(4)	7.8892(4)	8.5429(3)	90	104.926(4)	90	659.1(3)
11.13	10.1155(4)	7.8877(5)	8.5405(2)	90	104.907(2)	90	658.5(4)
12.05 [d]	10.0924(2)	7.8725(2)	8.5205(2)	90	104.856(2)	90	654.3(4)
12.08	10.0892(2)	7.8729(3)	8.51979(9)	90	104.832(2)	90	654.2(4)
			$CaSiO_3$-walstromite-III				
12.54 [d]	8.5111(2)	7.8542(3)	10.0964(3)	90	104.886(3)	90	652.3(4)
13.05	8.4985(2)	7.8294(2)	10.0985(2)	90	104.907(2)	90	649.3(4)
13.88 [d]	8.4813(2)	7.8018(3)	10.0916(3)	90	104.926(2)	90	645.2(4)
13.98	8.4769(3)	7.7959(4)	10.0874(4)	90	104.915(4)	90	644.2(4)
14.59 [d]	8.4636(3)	7.7752(4)	10.0787(3)	90	104.925(3)	90	640.9(4)
15.26	8.4534(2)	7.7631(3)	10.0734(3)	90	104.904(3)	90	638.8(4)
15.90	8.4396(2)	7.7443(2)	10.0622(2)	90	104.895(2)	90	635.6(3)
15.93 [d]	8.4419(2)	7.7435(2)	10.0682(2)	90	104.909(2)	90	636.0(3)
16.52 [d]	8.4306(2)	7.7280(3)	10.0587(3)	90	104.892(3)	90	633.3(3)
16.57	8.4288(2)	7.7282(2)	10.0544(2)	90	104.892(2)	90	632.9(3)
17.19	8.4187(2)	7.7133(2)	10.0479(2)	90	104.882(2)	90	630.6(3)
17.32 [d]	8.4196(2)	7.7112(3)	10.0512(3)	90	104.886(3)	90	630.7(3)
17.86	8.4078(2)	7.6983(2)	10.0405(2)	90	104.873(2)	90	628.1(3)
18.02 [d]	8.4014(3)	7.6884(4)	10.0342(4)	90	104.885(4)	90	626.4(3)
18.83	8.3921(3)	7.6763(4)	10.0280(4)	90	104.867(4)	90	624.4(3)
19.07 [d]	8.3860(3)	7.6658(5)	10.0214(5)	90	104.859(4)	90	622.7(3)
19.59	8.3815(3)	7.6598(4)	10.0196(4)	90	104.857(4)	90	621.8(3)
19.61 [d]	8.3786(3)	7.6551(4)	10.0163(4)	90	104.851(4)	90	621.0(3)
20.15	8.3756(3)	7.6512(4)	10.0147(4)	90	104.851(4)	90	620.3(3)

[d] Measurements in decompression.

The second phase transition, detected between 12–13 GPa, is a second-order phase transition, inasmuch the *V* decreased smoothly to the maximum pressure reached in the study of about 20 GPa with no noticeable volume discontinuity upon the $CaSiO_3$-walstromite-II to $CaSiO_3$-walstromite-III transition. The *P*–*V* data up to 8.5 GPa were fitted using a second-order Birch–Murnaghan EoS (BM2-EoS; [49]), since the Eulerian finite

strain (f_e) vs. normalized stress (F_e) plot of the data can be fitted by a horizontal straight line [50]. The BM2-EoS coefficients were refined simultaneously, data were weighted by their uncertainties in P and V, using the program EoSFit-7c [48] giving: V_0 = 375.9(4) Å^3, K_{T0} = 79(2) GPa and K' = 4 fixed (χ^2_w = 2.96). V data for 2nd and 3rd phase transitions, stable between 7.3–20.15 GPa decreases smoothly (Figure 5). The P–V data for $CaSiO_3$-walstromite-II and $CaSiO_3$-walstromite-III data were fitted using a BM2-EoS [49] using the program EoSFit-7c [48] giving K_{T0} = 101(6) GPa (K' = 4 fixed) and K_{T0} = 89(3) GPa (K' = 4 fixed) respectively.

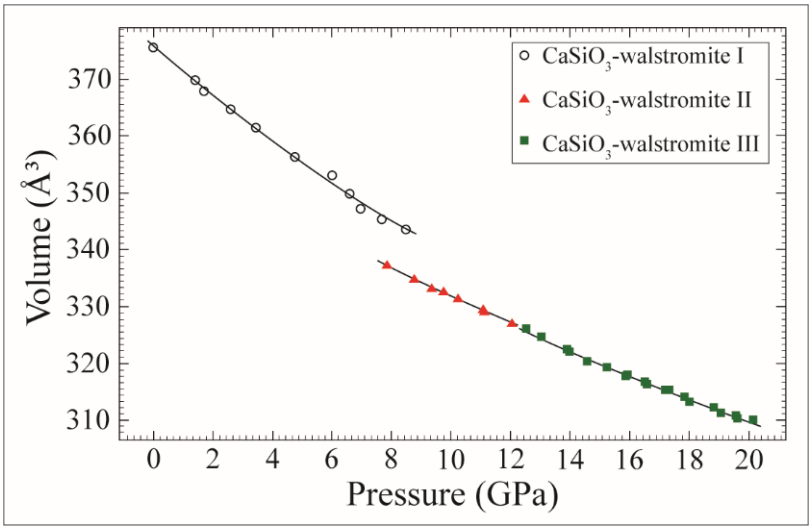

Figure 5. Evolution of the unit-cell volume with pressure of $CaSiO_3$-walstromite. Unit-cell volume data of the two HP polytypes have been normalized to the low-P polytype. The solid line represents the 2nd order BM-EoS fit.

The single crystal X-ray diffraction measurement confirms a triclinic lattice for $CaSiO_3$-walstromite-I. The refined unit-cell parameters are a = 6.6442(3), b = 6.886(4), c = 9.282(8) Å, α = 69.71(3), β = 83.68(2), γ = 76.205(5) and V = 375.6(3) Å^3 at ambient conditions and crystal structure refined in $P\bar{1}$ space group. The crystal structure determinations for $CaSiO_3$-walstromite-II and $CaSiO_3$-walstromite-III were successfully achieved in $C2/m$ and $P2_1/c$ space group respectively, using the crystallographic software Jana2006 [47]. The refined unit-cell constants for the three polytypes are listed in Table 4. The principal statistical parameters of the three structural refinements are listed in Table 5. Atomic coordinates, site occupancies of structure refinements and relevant bond distances are reported in Tables S3 and S4 while crystallographic information file is deposited as Supplementary Materials. $CaSiO_3$-walstromite structure is characterized by a repetition of a block, which is built as follows: the three ring Si-tetrahedra forms two 'chains' that are embedded and rotate for 180° (Figure 6a). This block is shifted in $CaSiO_3$-walstromite-II (Figure 6a,b). These changes are also visible on the volume changes of the 3 bigger polyhedral where Ca is located. $CaSiO_3$-walstromite has three large polyhedra: one is 6-coordinated, one is a 7 polyhedron, and the biggest one is a 7+1-coordinated polyhedron (Figure 2d). The two bigger polyhedra are characterized by a volume increase, while the bigger polyhedron is characterized by a volume decrease upon transition to $CaSiO_3$-walstromite-II. (Figure S3a,b). The second phase transition with no volume jump is due to a rotation of the silicate tetrahedra in the 3-fold rings, with consequent reduction of symmetry from $C2/m$ to $P2_1/c$ (Figure 6c).

Table 5. Details pertaining to the data collections and structure refinements of $CaSiO_3$-walstromite studied in this work.

Phase	$CaSiO_3$-Walstromite-I	$CaSiO_3$-Walstromite-II	$CaSiO_3$-Walstromite-III
a (Å)	6.6442(3)	10.2206(9)	8.5111(2)
b (Å)	6.6886(4)	7.9369(9)	7.8542(3)
c (Å)	9.282(8)	8.6213(7)	10.0964(3)
α (°)	69.71(3)	90	90
β (°)	83.68(2)	105.217(9)	104.886(3)
γ (°)	76.205(5)	90	90
V (Å^3)	375.6(3)	674.8(4)	652.3(4)
P (GPa)	0.0001(1)	9.37(5)	12.54(5)
Space group	$P\bar{1}$	$C2/m$	$P2_1/c$
λ (Å)	0.41105	0.41105	0.41105
θ_{max} (°)	19.18	19.76	19.11
No. measured reflections	890	699	1219
No. unique reflections	593	460	732
No. refined parameters	61	37	61
R_{int}	0.0301	0.083	0.047
R_1 (F)	0.0582	0.0498	0.0415
wR_2 (F^2)	0.0632	0.0594	0.0489
GooF	3.69	4.05	2.70
Residuals (e$^-$/Å^3)	−2.23/+5.77	−4.17/+5.29	-

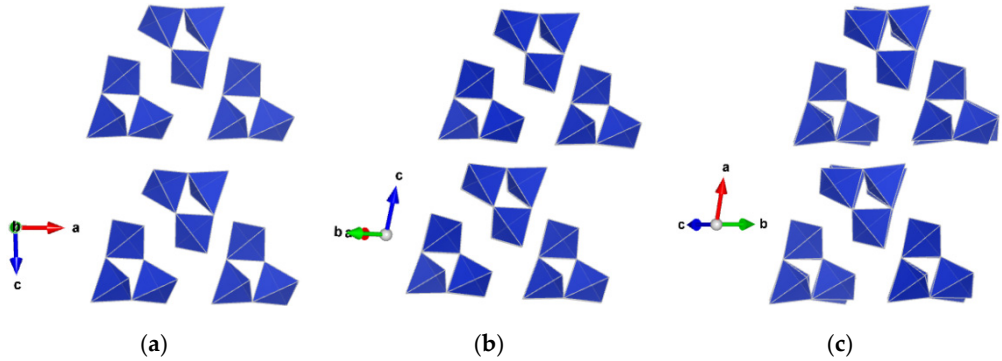

(**a**) (**b**) (**c**)

Figure 6. Phase transitions from (**a**) $CaSiO_3$-walstromite-I (**b**) $CaSiO_3$walstromite-II and (**c**) $CaSiO_3$-walstromite-III. The representations of the structure are realized using the program VESTA [17]; a axis is red, the green arrow is the b axis, while the blue arrow is the c axis.

4. Discussion and Conclusions

This study reports the elastic behavior of wollastonite and $CaSiO_3$-walstromite up to 22 GPa, showing for each mineral two structural phase transitions along the P ramps. Thermodynamic elastic parameters for these minerals are scarce in the literature. So far, only one experimental study on the P-V evolution of wollastonite has been published [52], where K_{T0} = 54.7 GPa. This value is much smaller with respect to what obtained in this study (K_{T0} = 93.9 GPa). This difference might be related to the increased accuracy achieved with the state of art of synchrotron experiments and the intrinsic greater accuracy in lattice parameter determination of the triclinic phase with a single crystal approach [42,53–55], compared to pioneering high-pressure measurements a few decades ago. The elastic parameters of wollastonite-II shows that this polytype is more compressible with respect to the low-pressure one. The bulk modulus value for $CaSiO_3$-walstromite determined in this study (K_{T0} = 79 (2)) agrees with the already published value of K_{T0} = 78.6 (1.3) [33]. $CaSiO_3$-waltrsomite-II and -III are less compressible (K_{T0} = 101(6) and 89(3) GPa respectively). From a thermodynamic point of view, the observed high-pressure wollastonite polytypes are likely metastable since they occur in the P-T space where $CaSiO_3$ ring-structures or perovskite structures are expected. $CaSiO_3$-walstromite-II, on the contrary, might be stable at some P-T conditions in the mantle, but accurate in-situ investigations are needed to verify this hypothesis and determine the stability field, given the unquenchable and

reversible nature of $CaSiO_3$-walstromite-II to -III transition. We in fact observed the back-transformation of $CaSiO_3$-walstromite on decompression, with a small hysteresis.

The structural modification of wollastonite and $CaSiO_3$-walstromite polytypes reveal, finally, interesting crystal-chemical features which applies to these topologies. With a minor deformation of the structural chains or rings possible to modify the elasticity of large cation sites in these structures, the displacement and packing of building blocks change the structures of the cation sites in terms of coordination number, as well as give a significant modulation of density. Furthermore, high-pressure polymorphs also increase the difference in terms of both size and elasticity of all the coordination sites other than tetrahedral silicate units. We performed experiments on pure $CaSiO_3$ compositions, but we may expect that the observed variations are compatible with compositions other than pure $CaSiO_3$. These observations can be likely transferred to possible analogue topologies, such as the predicted and observed high-pressure carbonate structures at deep-mantle conditions, above 80 GPa [8], where the carbon cation changes its coordination from three to four [13,14,56,57]. To date, no systematic investigations have been performed on high-pressure carbonates due to difficulties in synthesis of minerals at such extreme conditions and the limited accuracy of both theoretical and, especially, experimental studies at Mbar conditions. If we consider the evolution of the above-described structures for $CaSiO_3$ polymorphs and we compare them to the tetrahedrally coordinated carbonates we could conclude that threefold-ring carbonates [13] or truncated chain carbonates [58] might also increase their density through first-order phase transitions. We may similarly expect a rich polymorphism for these rather complex structures, and it is not unlikely that tetrahedrally coordinated carbon bearing carbonates may exist over a wide compositional range, including continuous solid solutions involving cations with different size (Ca vs. Mg in particular) and important minor or trace elements incorporation.

Supplementary Materials: The following are available online at https://www.mdpi.com/article/10.3390/min11060652/s1, Figure S1: Volume change of the bigger wollastonite polyhedra. (a) 7-fold coordination polyhedron; (b,c) 6-fold coordinated polyhedron. Figure S2: In-situ pictures of the pressure chamber loaded with a single crystal of $CaSiO_3$-walstomite, rubies as pressure standard and He as pressure transmitting medium. From the sequence of pictures, it is evident how the crystal 'jumps' from the center of the pressure chamber to the left margin. A movement is visible also in decompression, Figure S3: Volume change of the bigger $CaSiO_3$-walstromite polyhedra. (a) 6-fold coordinated polyhedron; (b) 7-fold coordination polyhedron (c) 7+1-fold coordination polyhedron. Table S1: Atomic coordinates, site occupancies and isotropic displacement parameters ($Å^2$) of the wollastonite studied in this work, Table S2: Interatomic distances (Å) selected from the structural refinement of the wollastonite studied in this work, Table S3: Atomic coordinates, site occupancies and isotropic displacement parameters ($Å^2$) of the $CaSiO_3$-walstromite studied in this work, Table S4: Interatomic distances (Å) selected from the structural refinement of the $CaSiO_3$-walstromite studied in this work. The CIF files are available as supplementary material.

Author Contributions: S.M. and M.M. conceived the study. S.M., D.C., P.L., P.F., L.Z., J.M., M.H. and M.M. performed the experiments, preliminary data analysis and discuss the results. S.M. and M.M. performed structure determinations and wrote the paper. All the authors revised the manuscript. All authors have read and agreed to the published version of the manuscript.

Funding: We acknowledge the support of the Italian Ministry of Education (MIUR) through the project 'Dipartimenti di Eccellenza 2018–2022'.

Data Availability Statement: Data is contained within the article or Supplementary Materials.

Acknowledgments: Andrea Risplendente for microprobe analysis, Michele Buono for technical support in experimental activities. European Synchrotron Radiation Facility is acknowledged for provision of beamtime at ID15B beamline. Ines Collings is thanked for technical support during beamtime at ID15B.

Conflicts of Interest: The authors declare no conflict of interest.

References

1. Palme, H.; Lodders, K.; Jones, A. Solar System Abundances of the Elements. In *Planets, Asteroids, Comets and the Solar System, Treatise on Geochemistry*, 2nd ed.; Davis, A.M., Ed.; Elsevier Ltd.: Amsterdam, The Netherlands, 2014; Volume 1, pp. 15–36.
2. McDonough, W.F. Compositional Model for the Earth's Core. In *The Mantle and Core, Treatise on Geochemistry*; Carlson, R.W., Ed.; Elsevier-Pergamon: Oxford, UK, 2003; Volume 2, pp. 547–568.
3. Rudnick, R.L.; Gao, S. Composition of the continental crust. In *The Crust, Treatise on Geochemistry*; Rudnick, R.L., Ed.; Elsevier-Pergamon: Oxford, UK, 2003; Volume 3, pp. 1–64.
4. Palme, H.; O'Neill, H.S.C. Cosmochemical estimates of mantle composition. In *The Mantle and Core, Treatise on Geochemistry*; Carlson, R.W., Ed.; Elsevier-Pergamon: Oxford, UK, 2003; Volume 2, pp. 1–38.
5. Gasparik, T.; Wolf, K.; Smith, C.M. Experimental determination of phase relations in the $CaSiO_3$ system from 8 to 15 GPa. *Am. Mineral.* **1994**, *79*, 1219–1222.
6. Pearson, D.G.; Brenker, F.E.; Nestola, F.; McNeill, J.; Nasdala, L.; Hutchison, M.T.; Matveev, S.; Mather, K.; Silversmit, G.; Schmitz, S.; et al. Hydrous mantle transition zone indicated by ringwoodite included within diamond. *Nature* **2014**, *507*, 221–224. [CrossRef] [PubMed]
7. Nestola, F.; Korolev, N.; Kopylova, M.; Rotiroti, N.; Pearson, D.G.; Pamato, M.G.; Alvaro, M.; Peruzzo, L.; Gurney, J.J.; Moore, A.E.; et al. $CaSiO_3$ perovskite in diamond indicates the recycling of oceanic crust into the lower mantle. *Nature* **2018**, *555*, 237–241. [CrossRef] [PubMed]
8. Holtstam, D.; Cámara, F.; Karlsson, A. Instalment of the margarosanite group, and data on walstromite-margarosanite solid solutions from the Jakobsberg Mn-Fe deposit, Värmland, Sweden. *Mineral. Mag.* **2021**, *85*, 224–232. [CrossRef]
9. Ringwood, A.E.; Major, A. Some high-pressure transformations of geophysical significance. *Earth Planet. Sci. Lett.* **1967**, *2*, 106–110. [CrossRef]
10. Oganov, A.R.; Hemley, R.J.; Hazen, R.M.; Jones, A.P. Structure, Bonding, and Mineralogy of Carbon at Extreme Conditions. In *Carbon in Earth, Reviews in Mineralogy and Geochemistry*; Hazen, R.M., Jones, A.P., Baross, J.A., Eds.; The Mineralogical Society of America: Chantilly, VA, USA, 2013; Volume 75, pp. 47–77.
11. Brenker, F.E.; Vollmer, C.; Vincze, L.; Vekemans, B.; Szymanski, A.; Janssens, K.; Szaloki, I.; Nasdala, L.; Joswig, W.; Kaminsky, F. Carbonates from the lower part of transition zone or even the lower mantle. *Earth Planet. Sci. Lett.* **2007**, *260*, 1–9. [CrossRef]
12. Hazen, R.M.; Hemley, R.J.; Mangum, A.J. Carbon in Earth's Interior: Storage, Cycling, and Life. *Eos* **2012**, *93*, 17–18. [CrossRef]
13. Merlini, M.; Cerantola, V.; Gatta, G.D.; Gemmi, M.; Hanfland, M.; Kupenko, I.; Lotti, P.; Müller, H.; Zhang, L. Dolomite-IV: Candidate structure for a carbonate in the Earth's lower mantle. *Am. Mineral.* **2017**, *102*, 1763–1766. [CrossRef]
14. Pickard, C.J.; Needs, R.J. Structures and stability of calcium and magnesium carbonates at mantle pressures. *Phys. Rev. B* **2015**, *91*, 104101. [CrossRef]
15. Holland, T.J.B.; Powell, R. An improved and extended internally consistent thermodynamic dataset for phases of petrological interest, involving a new equation of state for solids. *J. Metamorph. Geol.* **2011**, *29*, 333–383. [CrossRef]
16. Deer, W.A.; Howie, R.A.; Zussman, J. *Rock-Forming Minerals*, 2nd ed.; Singlechain Silicates; Geological Society Publishing House: London, UK, 1997; Volume 2.
17. Momma, K.; Izumi, F. VESTA 3 for three-dimensional visualization of crystal, volumetric and morphology data. *J. Appl. Crystallogr.* **2011**, *44*, 1272–1276. [CrossRef]
18. Hesse, K.-F. Refinement of the crystal structure of wollastonite-2M (parawollastonite). *Z. Krist.* **1984**, *168*, 93–98. [CrossRef]
19. Yang, H.; Prewitt, C.T. On the crystal structure of pseudowollastonite ($CaSiO_3$). *Am. Mineral.* **1999**, *84*, 929–932. [CrossRef]
20. Schiavinato, G. Il Giacimento a wollastonite ed altri minerali di contatto presso Alpe Bazena (Adamello meridionale). *Mem. Ist. Geol. Padova* **1947**, *15*, 1–63.
21. Allen, E.T.; White, W.P.; Wright, F.E. On wollastonite and pseudo-wollastonite-polymorphic forms of calcium metasilicate. *Am. Jour. Sci.* **1906**, *21*, 89–108. [CrossRef]
22. Prewitt, C.T. Structure and Crystal Chemistry of Wollastonite and Pectolite. Ph.D. Thesis, Massachusetts Institute of Technology, Cambridge, MA, USA, 1962.
23. Peacock, M.A. On wollastonite and parawollastonite. *Am. J. Sci.* **1935**, *30*, 495–529. [CrossRef]
24. Ito, T. *X-ray Studies on Polymorphism*; Maruzen: Tokyo, Japan, 1951; pp. 93–110.
25. Wenk, H.-R. Polymorphism of wollastonite. *Contrib. Mineral. Petrol.* **1969**, *22*, 238–247. [CrossRef]
26. Hutchison, J.L.; McLaren, A.C. Two-dimensional lattice images of stacking disorder in wollastonite. *Contrib. Mineral. Petrol.* **1976**, *55*, 303–309. [CrossRef]
27. Henmi, C.; Kawahara, A.; Henmi, K.; Kusachi, I.; Takeuchi, Y. The 3 T, 4 T and 5 T polytypes of wollastonite from Kushiro, Hiroshima Prefecture, Japan. *Am. Mineral.* **1983**, *68*, 156–163.
28. Seryotkin, Y.V.; Sokol, E.V.; Kokh, S.N. Natural pseudowollastonite: Crystal structure, associated minerals, and geological context. *Lithos* **2012**, *134–135*, 75–90. [CrossRef]
29. Stoppa, F.; Sharygin, V.V. Melilitolite intrusion and pelite digestion by high temperature kamafugitic magma at Colle Fabbri, Spoleto, Italy. *Lithos* **2009**, *112*, 306–320. [CrossRef]
30. Ingrin, J. TEM imaging of polytypism in pseudowollastonite. *Phys. Chem. Miner.* **1993**, *20*, 56–62. [CrossRef]
31. Brenker, F.; Nestola, F.; Brenker, L.; Peruzzo, L.; Secco, L.; Harris, J.W. Breyite, IMA 2018-062, CNMNC Newsletter. *Mineral. Mag.* **2018**, *82*, 1225–1232.

32. Brenker, F.E.; Vincze, L.; Vekemans, B.; Nasdala, L.; Stachel, T.; Vollmer, C.; Kersten, M.; Somogyi, A.; Adams, F.; Joswig, W. Detection of a Ca-rich lithology in the Earth's deep (>300 km) convecting mantle. *Earth Planet. Sci. Lett.* **2005**, *236*, 579–587. [CrossRef]
33. Anzolini, C.; Angel, R.J.; Merlini, M.; Derzsi, M.; Tokar, K.; Milani, S.; Krebs, M.Y.; Brenker, F.E.; Nestola, F.; Harris, J.W. Depth of formation of $CaSiO_3$ -walstromite included in super-deep diamonds. *Lithos* **2016**, *265*, 138–147. [CrossRef]
34. Brenker, F.E.; Nestola, F.; Brenker, L.; Peruzzo, L.; Harris, J.W. Origin, properties, and structure of breyite: The second most abundant mineral inclusion in super-deep diamonds. *Am. Mineral.* **2021**, *106*, 38–43. [CrossRef]
35. Woodland, A.B.; Girnis, A.V.; Bulatov, V.K.; Brey, G.P.; Hofer, H.E. Breyite inclusions in diamond: Experimental evidence for possible dual origin. *Eur. J. Mineral.* **2020**, *32*, 171–185. [CrossRef]
36. Joswig, W.; Paulus, E.F.; Winkler, B.; Milman, V. The crystal structure of $CaSiO_3$ -walstromite, a special isomorph of wollastonite-II. *Z. Krist.* **2003**, *218*, 811–818. [CrossRef]
37. Bulanova, G.P.; Smith, C.B.; Blundy, J.; Walter, M.J.; Kohn, S.C.; Gobbo, L.; Armstrong, L.S. Mineral inclusions in sublithospheric diamonds from Collier 4 kimberlite pipe, Juina, Brazil: Subducted protoliths, carbonated melts and primary kimberlite magmatism. *Contrib. Mineral. Petrol.* **2010**, *160*, 489–510. [CrossRef]
38. Trojer, F.J. The crystal structure of a high-pressure polymorph of $CaSiO_3$. *Z. Krist.* **1969**, *130*, 185–206. [CrossRef]
39. Barkley, M.C.; Downs, R.T.; Yang, H. Structure of walstromite, $BaCa_2Si_3O_9$, and its relationship to $CaSiO_3$-walstromite and wollastonite-II. *Am. Mineral.* **2011**, *96*, 797–801. [CrossRef]
40. Hamilton, D.L.; Henderson, C.M.B. The preparation of silicate composition by gelling method. *Mineral. Mag.* **1968**, *36*, 832–838. [CrossRef]
41. Fumagalli, P.; Poli, S. Experimentally determined phase relations in hydrous peridotites to 6.5 GPa and their consequences on the dynamics of subduction zones. *J. Petrol.* **2005**, *46*, 555–578. [CrossRef]
42. Merlini, M.; Hanfland, M. Single crystal diffraction at megabar conditions by synchrotron radiation. *High Press. Res.* **2013**, *33*, 511–522. [CrossRef]
43. Mao, H.K.; Xu, J.; Bell, P.M. Calibration of the ruby pressure gauge to 800 kbar under quasi-hydrostatic conditions. *J. Geophys. Res.* **1986**, *91*, 4673–4676. [CrossRef]
44. Chervin, J.C.; Canny, B.; Mancinelli, M. Ruby-spheres as pressure gauge for optically transparent high pressure cells. *High Press. Res.* **2001**, *21*, 305–314. [CrossRef]
45. Klotz, S.; Chervin, J.-C.; Munsch, P.; Le Marchand, G. Hydrostatic limits of 11 pressure transmitting media. *J. Phys. D.* **2009**, *42*, 075413. [CrossRef]
46. Rigaku Oxford Diffraction. *CrysAlisPro Software System*; Version 1.171.40.67a (2019); Rigaku Corporation: Wroclaw, Poland, 2019.
47. Petricek, V.; Dusek, M.; Palatinus, L. Crystallographic Computing System JANA2006: General features. *Z. Krist.* **2014**, *229*, 345–352.
48. Angel, R.J.; Gonzales-Platas, J.; Alvaro, M. EoSFit7c and a Fortran module (library) for equation of state calculations. *Z. Krist.* **2014**, *229*, 405–419. [CrossRef]
49. Birch, F. Finite elastic strain of cubic crystals. *Phys. Rev.* **1947**, *71*, 809–824. [CrossRef]
50. Angel, R.J. Equations of state. In *High-Temperature and High-Pressure Crystal Chemistry, Reviews in Mineralogy and Geochemistry*; Hazen, R.M., Downs, R.T., Eds.; Mineralogical Society of America: Chantilly, VA, USA, 2000; Volume 41, pp. 35–59.
51. Skoko, Ž.; Zamir, S.; Naumov, P.; Bernstein, J. The Thermosalient Phenomenon. "Jumping Crystals" and Crystal Chemistry of the Anticholinergic Agent Oxitropium Bromide. *J. Am. Chem. Soc.* **2010**, *132*, 14191–14202. [CrossRef] [PubMed]
52. Vaiday, S.N.; Bailey, S.; Pasternack, T.; Kennedy, G.C. Compressibility of fifteen minerals to 45 kilobars. *J. Geophys. Res.* **1973**, *78*, 6893–6898. [CrossRef]
53. Dera, P. All Different Flavors of Synchrotron Single Crystal X-ray Diffraction Experiments. In *High-Pressure Crystallography*; NATO Science for Peace and Security Series B: Physics and Biophysics; Boldyreva, E., Dera, P., Eds.; Springer: Dordrecht, The Netherlands, 2010; pp. 11–22.
54. Rothkirch, A.; Gatta, G.D.; Meyer, M.; Merkel, S.; Merlini, M.; Liermann, H.-P. Single-crystal diffraction at the Extreme Conditions beamline P02.2: Procedure for collecting and analyzing high-pressure single-crystal data. *J. Synchrotron Radiat.* **2013**, *20*, 711–720. [CrossRef] [PubMed]
55. Lotti, P.; Milani, S.; Merlini, M.; Joseph, B.; Alabarse, F.; Lausi, A. Single-crystal diffraction at the high-pressure Indo-Italian beamline Xpress at Elettra, Trieste. *J. Synchrotron Radiat.* **2020**, *27*, 222–229. [CrossRef]
56. Oganov, A.R.; Glass, C.W.; Ono, S. High-pressure phases of $CaCO_3$: Crystal structure prediction and experiment. *Earth Planet. Sci. Lett.* **2006**, *241*, 95–103. [CrossRef]
57. Boulard, E.; Pan, D.; Galli, G.; Liu, Z.; Mao, W.L. Tetrahedrally coordinated carbonates in Earth's lower mantle. *Nat. Comm.* **2015**, *6*, 6311. [CrossRef]
58. Cerantola, V.; Bykova, E.; Kupenko, I.; Merlini, M.; Ismailova, L.; McCammon, C.; Bykov, M.; Chumakov, A.I.; Petitgirard, S.; Kantor, I.; et al. Stability of iron-bearing carbonates in the deep Earth's interior. *Nat. Comm.* **2017**, *8*, 15960. [CrossRef]